RSC Advances

PAPER

View Article Online
View Journal | View Issue

Cite this: *RSC Adv.*, 2021, **11**, 39087

Strain in a platinum plate induced by an ultrahigh energy laser boosts the hydrogen evolution reaction†

Yuqian Huang,[a] Zhiguo Ye,[a]* Feng Pei,[b] Guang Ma,[c] Xinyuan Peng[a] and Duosheng Li[a]

The ligand and the strain near the active sites in catalysts jointly affect the electrocatalytic activity for the catalytic industry. In many cases, there is no effective strategy for the independent study of the strain effect without the ligand effect on the electrocatalytic activity for the hydrogen evolution reaction (HER). Laser shock peening (LSP) with a GW cm^{-2} level power density and a 10–30 ns short pulse is employed to form compressive strain on the surface and in the depth direction of a platinum (Pt) plate, which changes the inherent interatomic distance and modifies the energy level of the bonded electrons, thereby greatly optimizing the energy barrier for the HER. The crystal lattice near the surface of the LSP Pt plate is distorted by the strain, and the interplanar spacing decreases from 0.225 nm in the undeformed region to 0.211 nm in the deformed region. The specific activity of the LSP Pt has an increase of 2.9 and 6.4 times in comparison with that of the pristine Pt in alkaline and acidic environments, respectively. This investigation provides a novel strategy for the independent study of the strain effect on the electrocatalytic activity and the improvement of electrocatalysts with high performance in extensive energy conversion.

Received 6th September 2021
Accepted 29th November 2021

DOI: 10.1039/d1ra06688a

rsc.li/rsc-advances

1. Introduction

The destruction of the environment and the exhaustion of energy resources make the development of new energy extremely urgent.[1] Hydrogen energy, as a clean source, and its storage and transportation system are relatively complete; hydrogen energy has many other advantages, so scientific research on electrolysis of water to produce hydrogen has rapidly developed.[2–5] Currently, research on HER electrodes mainly focuses on precious metals and transition metal materials. In alkaline and acidic environments, the hydrogen evolution performance of Pt and its composite materials exhibits an absolute advantage. However, the rare reserves and high cost of precious metals hamper the HER at a large scale.[6,7] Therefore, transition metal alloys, oxides, nitrides, carbides, sulfides, borides and selenides have also been extensively studied for their excellent catalytic properties and bargain prices.[8–11] In terms of designing high-performance and low-cost electrocatalysts more and more technologies have been applied to develop the underlying electrocatalysts, such as cropping the interface structure and controlling the particle size, shape, size, composition and defects.[12,13]

Owing to the intrinsically sluggish kinetics of the HER, the efficiency of hydrogen production is subject to overpotential and stability.[14–16] In recent years, strain engineering has rapidly developed, it has proven to be an effective means of modifying the electronic structure and catalytic properties of nanomaterials, thus it will have a realistic significance to general application in engineering practice.[17–19] You *et al.* introduced the basic principle of the water decomposition reaction, putting forward a reasonable method of adjusting an electrocatalyst *via* mechanical strain and discussed the strain of the electrocatalyst, which has promoted research progress in recent years.[19] Familiar preparation methods of strain-effected structures generally include seed-mediated growth, galvanic replacement, electrochemical dealloying, and thermal annealing induced segregation.[20–24] Du's team used the physical technology of liquid laser ablation to produce a high density stacking defect in silver nanoparticles. The study found that the stacking defect would lead to a low coordination number and a high tensile strain that would commonly ameliorate the adsorption energy and transform the inactive silver into an active catalyst.[25] Guo and coworkers confirmed that compressive strain is applied to the atoms on a Pt surface, which weakens the binding to the intermediates of oxygen-containing reaction and slightly weakens the electrocatalytic activity of Pt

[a]*School of Material Science and Engineering, Nanchang Hangkong University, 696#, Feng HeNan Road, Nanchang 330063, China. E-mail: 70125@nchu.edu.cn*
[b]*State Grid JiangXi Electric Power Research Institute, Nanchang, 330096, China*
[c]*State Key Laboratory of Advanced Power Transmission Technology (Global Energy Interconnection Research Institute Co. Ltd), Beijing, 102209, China*

† Electronic supplementary information (ESI) available. See DOI: 10.1039/d1ra06688a

for oxygen reduction.[26] Zhe *et al.* designed strawberry-like structure with RhO_2 clusters embedded in the surface layer of Rh nanoparticles. The lattice mismatch between the RhO_2 cluster and Rh substrate causes intensive compressive strain which stabilizes the rhodium oxide on a low reduction potential.[27]

Herein, an ultrahigh energy laser with a GW cm^{-2} level power density and a 10–30 ns short pulse can produce a mass plasma shock wave for impacting Pt plates. Because Pt has good ductility, controllable strain can be obtained on the Pt plate surface by adjusting the power density of the ultrahigh energy laser. This method is more direct in studying the strain effect than the use of core–shell nanoparticle structures which may have uncertainties in the surface structure and surface area, preparation methods, particle size and distribution, and electronic structure effects.[4]

2. Materials and methods

2.1 Material preparation

Pure Pt plates (10 mm × 10 mm × 1 mm, >99.99%) were purchased from Xiyu Electromechanical Technology Co, Ltd (Shanghai, China). The surface of the Pt plates was impacted by a laser shock strengthening equipment (SGR-60-II) Nd:YAG laser at an operating power density of 3.5 GW cm^2 with a laser spot overlapping rate of 50% every scan time. During LSP, 0.1 mm special aluminium foil was employed as a laser energy absorption layer to improve the laser energy absorption and inhibit burning of the surface of the Pt plate. Water with a thickness of 1–2 mm was used as a constraint layer to prevent plasma expansion, increasing the peak value of the pressure and operation time of the shock wave.[28,29] The LSP diagram is shown in Fig. 1a. Before the impact test, the samples were polished and placed into beakers containing acetone and ethanol and then cleaned by ultrasonication.

2.2 Microstructure analysis

A stress tester (X'Pert-PRO MPD, Holland Panalytical) was employed to measure the residual stresses of the specimen (10 mm × 10 mm × 1 mm) with the $\sin^2\psi$ method.[30,31] The measurement used Cu Kα as radiation source ($\lambda = 0.154$ nm) at 40 kV and 40 mA with the inclination angles of 0°, 10°, 15°, 25°, 30°, 40° and 45° at a step length of 0.02° s^{-1}. The microstructures of all the specimens were tested by transmission electron microscopy (TEM, FEI Talos F200S A-TWIN) and energy-dispersive X-ray spectroscopy (EDS, Oxford Instruments). X-ray diffraction (XRD, Bruker D8 ADVANCE) was employed to analyze their phase and structure. The field emission scanning electron microscope (FESEM) images were performed on FEI Nova Nano SEM 450 at an acceleration voltage of 15 kV. To identify the chemical compositions and electronic states, X-ray photoelectron spectroscopy (XPS, XPSINCA 250 X-max 50) was performed. The hardness of the sample section was tested by Digital Micro Vickers hardness tester (SCTMC, HVS-1000Z). The surface roughness and profile of samples before and after LSP were obtained by roughness profiler (JB-6C).

2.3 Electrode performance

All electrochemical experiments were measured at 25 °C using an electrochemical workstation (CHI-660C, Shanghai CHI Instruments, Inc.) under a standard three-electrode system in a 0.5 M H_2SO_4 medium and 1.0 M KOH medium, respectively. The sample, a saturated calomel electrode (SCE) (see Fig. S1†) and a graphite rod were employed as the working electrode, reference electrode, and counter electrode in a 0.5 M H_2SO_4 medium, respectively. Similarly, a Hg/HgO electrode[32] were employed as the reference electrode in a 1.0 M KOH medium. All the tested potentials were converted to a reversible hydrogen electrode (RHE). Linear sweep voltammetry (LSV) curves of all the samples were measured at a scan rate of 1 mV s^{-1}. Electrochemical impedance spectroscopy (EIS) was carried out at a HER potential of 91.3 mV and 236 mV over the frequency range of 100 000–0.01 Hz with 5 mV amplitude in acidic and alkaline medium, respectively.

The polarization curves were *iR*-compensated using the following E_q:

$$E_c = E_m - iR_s \quad (1)$$

where E_c represents the corrected potential, E_m is the measured potential and R_s denotes as the resistance of the solution.

3. Results and discussion

Laser shock peening (LSP) with an ultrahigh power density and an ultrashort pulse is employed for the first time for the fabrication of a strained Pt plate without the ligand effect. Fig. 1b shows the residual stress on the surface of pristine and LSP Pt plates. As shown in Fig. 1b, LSP Pt plates possess a higher residual stress (270.6 MPa) than the pristine Pt plate (93.2 MPa), indicating the existence of mass compressive strain on the LSP Pt plate. The depth of the effect of LSP on Pt plate is estimated 250 μm by the hardness fluctuation of the sample section along the depth direction,[33] 11 points along the depth direction of LSP Pt plate were tested and plotted as a graph Fig. 1c. Fig. S2† exhibits the surface roughness values (R_a) and surface morphologies of pristine Pt and LSP Pt plates. As shown in the Fig. S2a and b,† the LSP Pt plate has a higher R_a value of 0.452 μm than the pristine one of 0.107 μm. The surface of the LSP sample formed many obvious pits owing to the violent impact (see Fig. S2c and d†).

Fig. 1d exhibits the XRD patterns of pristine Pt and LSP Pt plates. As seen in Fig. 1d, the (111), (200) and (220) facets of the pristine Pt plate correspond to the diffraction peaks at 39.67°, 46.16° and 67.35° (JCPDS no. 04-0802), respectively, from which a lattice parameter of 3.924 Å is calculated. Similarly, the (111), (200) and (220) facets of the LSP Pt plate correspond to the diffraction peaks at 39.74°, 46.20° and 67.41°, respectively, indicating a small decrease in the lattice parameter after applying LSP on the surface of the pristine Pt plate. Moreover, the three strong peaks of the LSP Pt plate shift towards larger angles compared to the pristine Pt plate, indicating a decrease in the interplanar spacing, which is consistent with the change in the lattice parameter. There is also a relative variation in the

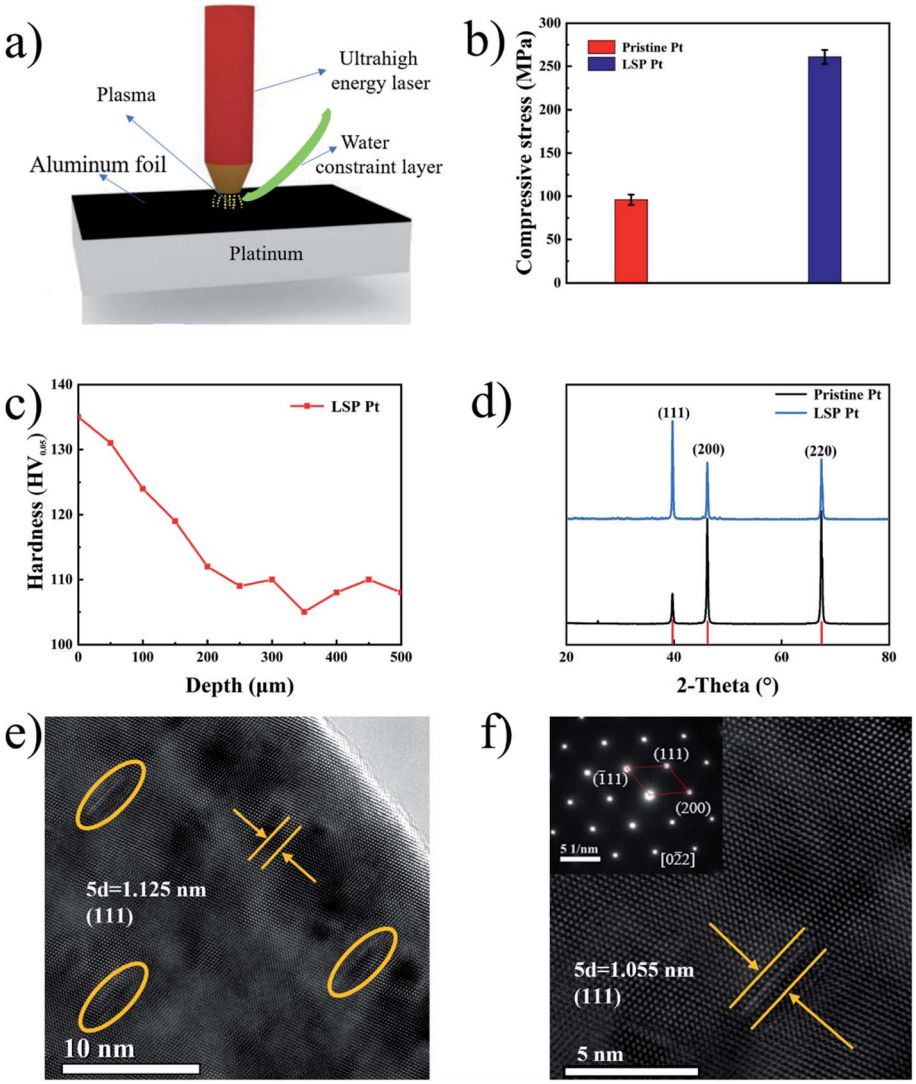

Fig. 1 (a) Diagram of LSP of a pristine Pt plate. (b) Residual stresses and (d) XRD patterns of the electrode surfaces of pristine Pt and LSP Pt plates. (c) Cross-section hardness distribution curve of the LSP Pt. (e and f) HRTEM images of the LSP Pt plate. (f) Is the enlarged plot of the yellow circle in the upper left corner of (e).

diffraction peak intensity for the pristine and LSP Pt plates, which should be the consequence of a charge in the crystallographic orientation owing to the impact of ultrahigh energy laser on the sample surface. Obviously, the intensity ratio of the (111) to (200) and (220) facet in the LSP Pt is stronger than that of pristine, indicating a higher preferential degree in the crystalline orientation and more possibly exposed (111) facet on the LSP sample surface.[34] However, the electrocatalytic activity of the Pt (111) facet is lower than that of Pt (100) and Pt (110) facets in the acid and alkaline media in the reported ref. 35–40. Fig. 1e exhibits an HRTEM image of the LSP Pt plate. As shown in the figure, the LSP Pt plate in the undeformed region has an interplanar spacing of 0.225 nm as calculated by Digital Micrograph, corresponding to the (111) facet of pure Pt. Clearly, there are many deformed crystal lattices inside the grain near the surface owing to the impact of the ultrahigh energy in comparison with the pristine sample (Fig. S3†). The crystal lattice near the surface of the LSP Pt plate has an obvious distortion, and the interplanar spacing decreases from 0.225 nm in the undeformed region to 0.211 nm in the deformed region Fig. 1f, which is coincident with the XRD results. The LSP technique with an ultrahigh power density of the laser causes a mass compressive strain, lattice deformation near the Pt plate surface and a decrease in the interplanar spacing, thus greatly modifying the energy level of bonding electrons[2,25,41] and the energy barrier for the HER and accelerating the adsorption of hydrogen in water molecules on the surface of the electrode.[42–44]

Fig. 2a shows the LSV curves of pristine Pt and LSP Pt electrodes at a scan speed of 1 mV s^{-1} in a 0.5 M H_2SO_4 solution. As shown in the figure, the current density of 10 mA cm^{-2} is reached, the LSP Pt electrode has a lower potential (48 mV) than the pristine Pt electrode (79 mV), indicating higher electrocatalytic activity owing to the stain of LSP. To judge the

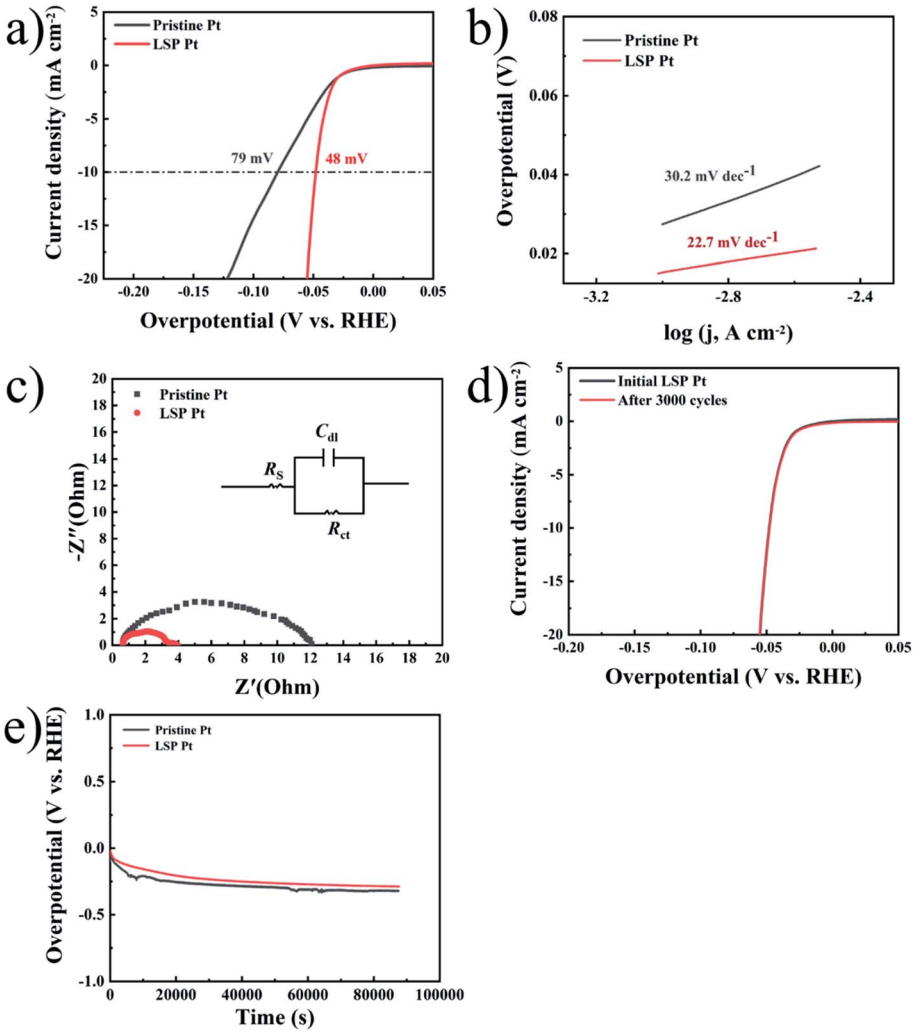

Fig. 2 (a) LSV curves of pristine Pt and LSP Pt electrodes in a 0.5 M H_2SO_4 solution. (b) Tafel plots of all electrodes with an iR_s correction obtained from the curves of Fig. 3(a). (c) Nyquist plots of the samples performed at an HER potential of 91.3 mV (*vs.* RHE) over a frequency range of 100 000–0.01 Hz. (d) Corresponding polarization curves of LSP electrode before and after 3000 CV cycles. (e) Stability test of pristine Pt and LSP Pt electrodes at a fixed current density of 10 mA cm^{-2} in a 0.5 M H_2SO_4 medium.

hydrogen evolution kinetics, the Tafel slope and EIS data are usually employed as important indicators to evaluate the kinetics and reveal the HER mechanism.[45,46] The main ways of HER can be divided into Volmer–Tafel or Volmer–Heyrovsky, because of the different rate determination steps (RDS), HER has four different mechanisms and Tafel slopes, corresponding to Volmer (RDS)–Heyrovsky (118 mV dec^{-1}), Volmer–Heyrovsky (RDS) (39 mV dec^{-1}), Volmer (RDS)–Tafel (118 mV dec^{-1}), Volmer–Tafel (RDS) (30 mV dec^{-1}). The Tafel plots of electrodes are employed a 95% iR_s correction. Fig. 2b shows the Tafel slope (22.7 mV dec^{-1}) of the LSP Pt electrode is lower than the pristine Pt electrode (30.2 mV dec^{-1}), further demonstrating the LSP action on electrocatalytic activity. Undoubtedly, these consequences are comparative with the advanced electrocatalysts for the HER (see Table S3†). The Tafel plots of the pristine and LSP Pt plates indicate the consistency with the Volmer–Tafel mechanism in an acidic medium. The results also are consistent with Tian *et al.*,[47] who proved that the HER mechanism is the same on Pt in low and high pH.[48] From the analysis of the above hydrogen evolution kinetics, it can be known that the RDS of the HER reaction, so it can be guessed that the strain effect improves the HER kinetic constant on the surface of electrodes and reduces the adsorption energy.[49]

The EIS data obtained from 100 kHz to 0.01 Hz at a tested overpotential of 91.3 mV is analyzed by using the equivalent circuit ($R_s(C_{dl}R_{ct})$), as displayed in Fig. 2c. R_s denotes as the solution resistance C_{dl} represents double-layer capacitance and R_{ct} is charge-transfer resistance during the HER process,[50] as displayed in Fig. 2c, the Nyquist profiles exhibit a semicircle that represents the HER kinetics in the electrode materials. The LSP Pt electrode has a lower R_{ct} of approximately 3.5 Ω cm^{-2} than that for the pristine Pt electrode of 9.2 Ω cm^{-2} (see Table S1†), indicating an increase of electrocatalytic activity owing the LSP impact.[51–53] Fig. 2d displays the polarization curves of LSP electrode before and after 3000 CV cycles. As seen in Fig. 2d, after 3000 CV cycles at a quite fast scan rate (100 mV s^{-1}), the

LSP Pt electrode shows negligible activity loss, indicating the outstanding stability. Fig. 2e displays the long-term stability of pristine Pt and LSP Pt electrodes at a fixed current density of 10 mA cm^{-2} in a 0.5 M H_2SO_4 medium. With an increase of time, the potentials of pristine Pt and LSP Pt electrodes gradually decrease owing to a bubble accumulation on the electrode surface and then remain stable during the succedent HER process. Obviously, the LSP Pt electrode possesses a lower overpotential of the HER than pristine Pt, indicating the more excellent electrocatalytic activity and stability.

Similarly, Fig. 3a exhibits the LSV curves of pristine Pt and LSP Pt electrodes at a scan speed of 1 mV s^{-1} in a 1 M KOH solution. As shown in the figure, the LSP Pt electrode for a current density of 10 mA cm^{-2} has a lower potential (139 mV) than the pristine Pt electrode (264 mV), indicating higher electrocatalytic activity owing to the stain of LSP. In Fig. 3b, the Tafel slope (65.7 mV dec^{-1}) of the LSP Pt electrode is lower than the pristine Pt electrode (91.2 mV dec^{-1}), too. As shown in Fig. 3c and Table S2,† the LSP Pt electrode has a lower R_{ct} of approximately 4.4 Ω cm^{-2} than that for the pristine Pt electrode of 8.3 Ω cm^{-2} in alkaline medium, which is consistent with the electrode in acid solution. These consequences confirm that the LSP can improve the electrocatalytic activity of the Pt electrode in acid and alkaline medium.

The intrinsic activity should be further explored, specific activity, which is the current per unit real surface area of the electrocatalyst (*i.e.*, mA $cm_{electrocatalyst}^{-2}$ at a given HER potential), mainly depends on the calculation of the surface area.[54] The electrical double-layer capacitance (C_{dl}) is directly proportional to the electrochemically active surface area (ECSA), which is often employed to evaluate the ECSA by calculating the cyclic voltammetry (CV) data (see Fig. S4†). The ECSA can be estimated by:

$$\mathrm{ECSA} = \frac{C_{dl}}{C^{s}} \tag{2}$$

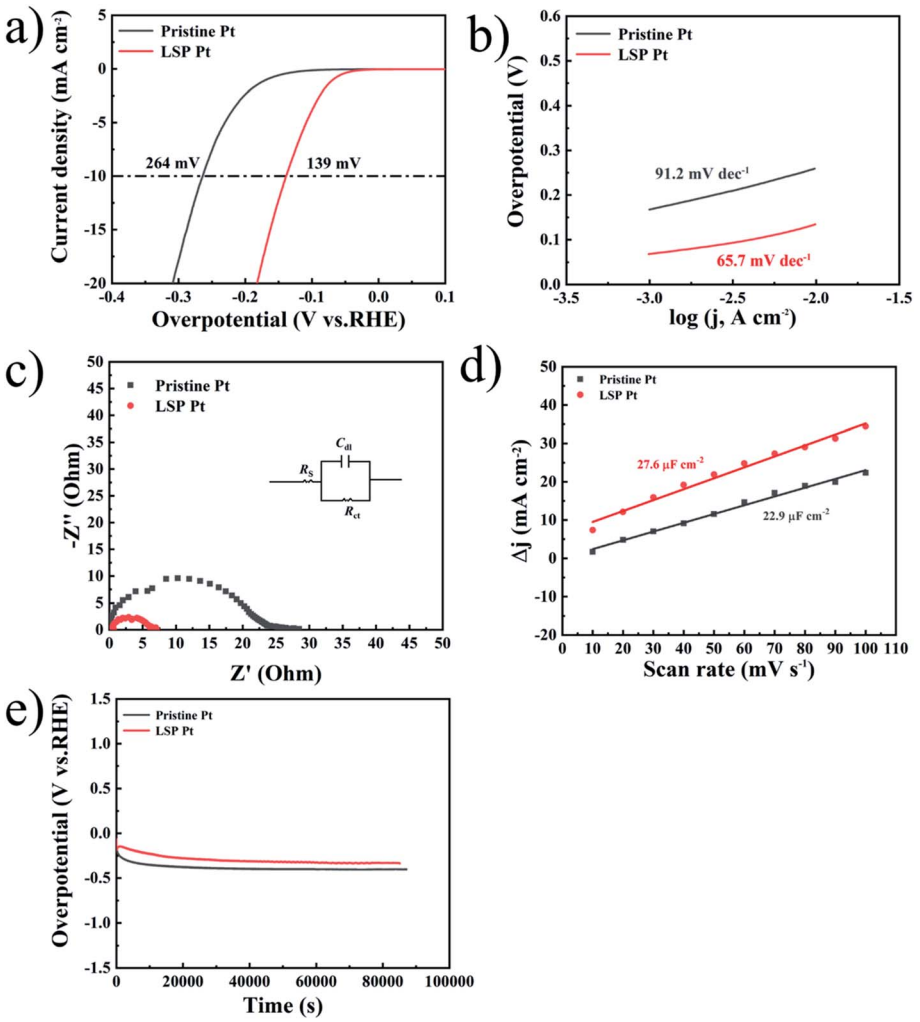

Fig. 3 (a) LSV curves of the pristine Pt and LSP electrodes in a 1 M KOH solution. (b) Tafel plots of all electrodes with an iR_s correction obtained from the curves of (a). (c) Nyquist plots of the samples performed at an HER potential of 225 mV (*vs.* RHE). (d) C_{dl} values of the pristine Pt and LSP electrodes measured in a 1 M KOH medium. (e) Stability test of the pristine Pt and LSP electrodes at a fixed current density of 10 mA cm^{-2} in a 1 M KOH medium.

where C^s is the specific capacitance of the double layer of the smooth Pt electrode. Fig. 3d shows that the C_{dl} values of the pristine Pt and LSP Pt electrodes reach 22.9 μF cm^{-2} and 27.6 μF cm^{-2}, respectively. According to the literature, the C^s of a smooth Pt electrode is approximately 20 μF cm^{-2},[55] as shown in Fig. 3d, the ECSA can be calculated as approximately 1.2 cm^2 and 1.4 cm^2, respectively. The specific activity can be calculated by applying the current densities at a HER potential of −0.3 V and −0.15 V (*vs.* RHE) in Fig. 3a and 2a, respectively, which are shown in Tables 1 and 2. In alkaline medium, the specific activities of pristine Pt and LSP Pt electrodes are 14.9 mA cm^{-2} and 43.2 mA cm^{-2}, respectively. In acidic medium, the LSP Pt electrode achieve a specific activity of 144.5 mA cm^{-2}, which is far higher than that of higher pristine Pt electrode (22.5 mA cm^{-2}). Obviously, the intrinsic activity of the LSP Pt has an increase of 2.9 and 6.4 times in comparison with that of the pristine Pt in alkaline and acidic environments, respectively, which should be attributed to the compressive strain derived from the LSP on the surface. The compressive strain near the surface of the LSP Pt plate changed the inherent interatomic distance and modified the energy level of the bonded electrons,[2,25,41] which can adjust the energy barrier of HER to accelerate the adsorption of hydrogen in water molecules on the surface of electrode.[42–44] From the analysis of the hydrogen evolution kinetics, it can be concluded that the strain reduces the adsorption energy and improves the HER on the surface of the LSP Pt plate.[56] Andrew A. Peterson and Pradeep R. Guduru *et al.*[57] confirmed that the influence of compression strain on the HER of Pt conforms to the volcano plot and d-bind theory *via* through theoretical experiments, corresponding to the above consequence. The compression strain near the surface of the LSP Pt plate increases the Pt d-band overlap and decreases the center of d-band, which can pull the antibonding state below the Fermi level and weaken the Pt surface's binding to adsorbents,[4,43,44,58] leading to a higher intrinsic electrocatalytic activity of the HER.

Fig. 3e displays the long-term stability of pristine Pt and LSP Pt electrodes at a fixed current density of 10 mA cm^{-2} in a 1 M KOH medium. As shown in the figure, the LSP Pt electrode possesses a lower overpotential under the long-term HER process, indicating more excellent electrocatalytic activity and stability in comparison with pristine Pt plate. The surface morphologies, composition, structure and valence state of species on the surface of unaged and aged LSP Pt electrodes for 24 hours at a fixed current density of 10 mA cm^{-2} in a 0.5 M H_2SO_4 and 1 M KOH solution have not a change, further indicating the superior stability of the LSP Pt plate for the HER (see Fig. S5–S7†).

Table 1 Summary of the calculated intrinsic activities of pristine Pt and LSP Pt electrodes in alkaline environment

Samples	C_{dl} (μF cm^{-2})	ECSA (cm^2)	Current (mA)	Specific activity (mA cm^{-2})
Pristine Pt	22.9	1.2	17.9	14.9
LSP Pt	27.6	1.4	60.5	43.2

Table 2 Summary of the calculated intrinsic activities of pristine Pt and LSP Pt electrodes in acidic environment

Samples	ECSA (cm^2)	Current (mA)	Specific activity (mA cm^{-2})
Pristine Pt	1.2	27.1	22.5
LSP Pt	1.4	202.3	144.5

4. Conclusion

In summary, LSP with an ultrahigh power density and an ultrashort pulse was successfully applied to achieve mass compressive strain and lattice deformation near the Pt plate surface. The interplanar spacing decreases from 0.225 nm in the undeformed region to 0.211 nm in the deformed region. The LSP Pt electrode has an increase of 3.5 and 6.8 times on the intrinsic activity in alkaline and acidic medium, respectively. This work opens a new door for independent strain investigations on the electrocatalytic activity and fabrication of novel electrocatalysts.

Author contributions

Zhiguo Ye: conceived the idea of this study and designed the experiments. Yuqian Huang: performed the sample synthesis, material characterizations and electrochemical measurements. Zhiguo Ye, Yuqian Huang, Feng Pei, Guang Ma, Xinyuan Peng, and Duosheng Li analysed the data and discussed the results. Zhiguo Ye and Yuqian Huang co-wrote and revised the manuscript.

Conflicts of interest

The authors declare that there are no known competing financial interests or personal relationships that could have appeared to influence the work reported in this paper.

Acknowledgements

Funding: this work was supported by the National Natural Science Foundation of China (51862026 and 51562027), the Aeronautical Science Foundation of China (2017ZF56027), the Natural Science Foundation of Jiangxi Province (20192ACBL21048), the State Grid Corporation of China Science and Technology Project (SGGR0000DWJS1901071), the Excellent Youth Foundation of Jiangxi Scientific Committee (20171BCB23054) and Key Research and Development Program of Jiangxi Province (20203BBE53069).

References

1 J. Chow, R. J. Kopp and P. R. Portney, *Science*, 2003, **302**, 1528–1531.
2 M. Mavrikakis, B. Hammer and J. K. Nørskov, *Phys. Rev. Lett.*, 1998, **81**, 2819–2822.

3 R. B. Patil, A. Mantri, S. D. House, J. C. Yang and J. R. McKone, *ACS Appl. Energy Mater.*, 2019, **2**, 2524–2533.
4 M. Du, L. Cui, Y. Cao and A. J. Bard, *J. Am. Chem. Soc.*, 2015, **137**, 7397–7403.
5 Z. Ye, T. Li, G. Ma, Y. Dong and X. Zhou, *Adv. Funct. Mater.*, 2017, **27**, 1–8.
6 G. Gao, Q. Sun and A. Du, *J. Phys. Chem. C*, 2016, **120**, 16761–16766.
7 J. Durst, C. Simon, F. Hasché and H. A. Gasteiger, *J. Electrochem. Soc.*, 2015, **162**, F190–F203.
8 L. Petry, E. Shin, D. C. Hansen, R. G. Keil and P. T. Murray, *Electrochim. Acta*, 2011, **56**, 6779–6788.
9 C. González-Buch, I. Herraiz-Cardona, E. Ortega, J. García-Antón and V. Pérez-Herranz, *J. Appl. Electrochem.*, 2016, **46**, 791–803.
10 Y. Zhang, Y. Wang, S. Jia, H. Xu, J. Zang, J. Lu and X. Xu, *Electrochim. Acta*, 2016, **222**, 747–754.
11 S. Kabir, K. Lemire, K. Artyushkova, A. Roy, M. Odgaard, D. Schlueter, A. Oshchepkov, A. Bonnefont, E. Savinova, D. C. Sabarirajan, P. Mandal, E. J. Crumlin, I. V. Zenyuk, P. Atanassov and A. Serov, *J. Mater. Chem. A*, 2017, **5**, 24433–24443.
12 R. Subbaraman, D. Tripkovic, D. Strmcnik, K. C. Chang, M. Uchimura, a P. Paulikas, V. Stamenkovic and N. M. Markovic, *Science*, 2011, **334**, 1256–1260.
13 I. Ledezma-Yanez, W. D. Z. Wallace, P. Sebastián-Pascual, V. Climent, J. M. Feliu and M. T. M. Koper, *Nat. Energy*, 2017, **2**, 1–24.
14 S. Liu, Z. Hu, Y. Wu, J. Zhang, Y. Zhang, B. Cui, C. Liu, S. Hu, N. Zhao, X. Han, A. Cao, Y. Chen, Y. Deng and W. Hu, *Adv. Mater.*, 2020, **2006034**, 1–8.
15 C. C. L. McCrory, S. Jung, J. C. Peters and T. F. Jaramillo, *J. Am. Chem. Soc.*, 2013, **135**, 16977–16987.
16 X. Zhao, P. Pachfule, S. Li, J. R. J. Simke, J. Schmidt and A. Thomas, *Angew. Chem., Int. Ed.*, 2018, **57**, 8921–8926.
17 B. T. Sneed, A. P. Young and C. K. Tsung, *Nanoscale*, 2015, **7**, 12248–12265.
18 C. Becher, L. Maurel, U. Aschauer, M. Lilienblum, C. Magén, D. Meier, E. Langenberg, M. Trassin, J. Blasco, I. P. Krug, P. A. Algarabel, N. A. Spaldin, J. A. Pardo and M. Fiebig, *Nat. Nanotechnol.*, 2015, **10**, 661–665.
19 B. You, M. T. Tang, C. Tsai, F. Abild-Pedersen, X. Zheng and H. Li, *Adv. Mater.*, 2019, **31**, 1–28.
20 P. Strasser, S. Koh, T. Anniyev, J. Greeley, K. More, C. Yu, Z. Liu, S. Kaya, D. Nordlund, H. Ogasawara, M. F. Toney and A. Nilsson, *Nat. Chem.*, 2010, **2**, 454–460.
21 S. Guo, S. Zhang, D. Su and S. Sun, *J. Am. Chem. Soc.*, 2013, **135**, 13879–13884.
22 M. Oezaslan, F. Hasché and P. Strasser, *J. Phys. Chem. Lett.*, 2013, **4**, 3273–3291.
23 L. Dubau, J. Nelayah, T. Asset, R. Chattot and F. Maillard, *ACS Catal.*, 2017, **7**, 3072–3081.
24 R. Chattot, T. Asset, P. Bordet, J. Drnec, L. Dubau and F. Maillard, *ACS Catal.*, 2017, **7**, 398–408.
25 Z. Li, J. Y. Fu, Y. Feng, C. K. Dong, H. Liu and X. W. Du, *Nat. Catal.*, 2019, **2**, 1107–1114.
26 L. Bu, N. Zhang, S. Guo, X. Zhang, J. Li, J. Yao, T. Wu, G. Lu, J. Y. Ma, D. Su and X. Huang, *Science*, 2016, **354**, 1410–1414.
27 Z. Li, Y. Feng, Y. L. Liang, C. Q. Cheng, C. K. Dong, H. Liu and X. W. Du, *Adv. Mater.*, 2020, **32**, 1–7.
28 M. Z. Ge and J. Y. Xiang, *J. Alloys Compd.*, 2016, **680**, 544–552.
29 M. G. Yin, Z. B. Cai, Z. Y. Li, Z. R. Zhou, W. J. Wang and W. F. He, *Trans. Nonferrous Met. Soc. China*, 2019, **29**, 1439–1448.
30 R. Gadallah, S. Tsutsumi, Y. Aoki and H. Fujii, *J. Manuf. Process.*, 2021, **64**, 1223–1234.
31 M. Vhareta, R. M. Erasmus and J. D. Comins, *Int. J. Refract. Met. Hard Mater.*, 2020, **88**, 105176.
32 J. Tang, J. L. Xu, Z. G. Ye, Y. C. Ma, X. B. Li, J. M. Luo and Y. Z. Huang, *J. Alloys Compd.*, 2021, **885**, 160995.
33 Y. Yang, K. Zhou and G. Li, *Opt. Laser Technol.*, 2019, **109**, 1–7.
34 Z. G. Ye, H. M. Meng, D. Chen, H. Y. Yu, Z. S. Huan, X. D. Wang and D. B. Sun, *Solid State Sci.*, 2008, **10**, 346–354.
35 N. M. Marković, B. N. Grgur and P. N. Ross, *J. Phys. Chem. B*, 1997, **101**, 5405–5413.
36 Z. Da He, J. Wei, Y. X. Chen, E. Santos and W. Schmickler, *Electrochim. Acta*, 2017, **255**, 391–395.
37 E. S. Davydova, S. Mukerjee, F. Jaouen and D. R. Dekel, *ACS Catal.*, 2018, **8**, 6665–6690.
38 T. J. Schmidt, V. Stamenkovic, P. N. Ross and N. M. Markovic, *Phys. Chem. Chem. Phys.*, 2003, **5**, 400–406.
39 J. H. Barber and B. E. Conway, *J. Electroanal. Chem.*, 1999, **461**, 80–89.
40 B. E. Conway and B. V. Tilak, *Electrochim. Acta*, 2002, **47**, 3571–3594.
41 J. Durst, A. Siebel, C. Simon, F. Hasché, J. Herranz and H. A. Gasteiger, *Energy Environ. Sci.*, 2014, **7**, 2255–2260.
42 A. Madram, M. Mohebbi, M. Nasiri and M. R. Sovizi, *Int. J. Hydrogen Energy*, 2020, **45**, 3940–3947.
43 A. Nilsson, L. G. M. Pettersson, B. Hammer, T. Bligaard, C. H. Christensen and J. K. Nørskov, *Catal. Lett.*, 2005, **100**, 111–114.
44 Y. Yang, T. Adit Maark, A. Peterson and S. Kumar, *Phys. Chem. Chem. Phys.*, 2015, **17**, 1746–1754.
45 S. Poorahong, D. J. Harding and M. Siaj, *Mater. Lett.*, 2020, **272**, 127872.
46 P. Wang, X. Zhang, J. Zhang, S. Wan, S. Guo, G. Lu, J. Yao and X. Huang, *Nat. Commun.*, 2017, **8**, 1–9.
47 X. Tian, P. Zhao and W. Sheng, *Adv. Mater.*, 2019, **31**, 1–7.
48 W. Sheng, Z. Zhuang, M. Gao, J. Zheng, J. G. Chen and Y. Yan, *Nat. Commun.*, 2015, **6**, 1–6.
49 J. Zheng, W. Sheng, Z. Zhuang, B. Xu and Y. Yan, *Sci. Adv.*, 2016, **2**, 1–9.
50 P. Shang, Z. Ye, Y. Ding, Z. Zhu, X. Peng, G. Ma and D. Li, *ACS Sustain. Chem. Eng.*, 2020, **8**, 10664–10672.
51 S. Asadi, A. R. Madram, E. Biglari, M. Fekri and F. Fotouhi-Far, *Int. J. Hydrogen Energy*, 2019, **44**, 8223–8232.
52 A. L. Bhatti, U. Aftab, A. Tahira, M. I. Abro, M. Kashif Samoon, M. H. Aghem, M. A. Bhatti and Z. Hussainibupoto, *RSC Adv.*, 2020, **10**, 12962–12969.
53 R. Subbaraman, D. Tripkovic, K. C. Chang, D. Strmcnik, A. P. Paulikas, P. Hirunsit, M. Chan, J. Greeley,

V. Stamenkovic and N. M. Markovic, *Nat. Mater.*, 2012, **11**, 550–557.

54 C. Wei, S. Sun, D. Mandler, X. Wang, S. Z. Qiao and Z. J. Xu, *Chem. Soc. Rev.*, 2019, **48**, 2518–2534.

55 T. Pajkossy and D. M. Kolb, *Electrochem. Commun.*, 2003, **5**, 283–285.

56 R. Djara, Y. Holade, A. Merzouki, N. Masquelez, D. Cot, B. Rebiere, E. Petit, P. Huguet, C. Canaff, S. Morisset, T. W. Napporn, D. Cornu and S. Tingry, *J. Electrochem. Soc.*, 2020, **167**, 066503.

57 K. Yan, T. A. Maark, A. Khorshidi, V. A. Sethuraman, A. A. Peterson and P. R. Guduru, *Angew. Chem., Int. Ed.*, 2016, **55**, 6175–6181.

58 J. R. Kitchin, J. K. Nørskov, M. A. Barteau and J. G. Chen, *Phys. Rev. Lett.*, 2004, **93**, 4–7.